DØNote 2493

Jet Production at Large Rapidity Intervals

Terry C. Heuring
Florida State University
Soon Yung Jun
Northwestern University
Chang Lyong Kim
Korea University

March 9, 1995

1 Introduction

The strategy of QCD measurements at hadron colliders has been to compare inclusive jet cross sections at relatively high p_T and small rapidities to leading order (LO) and next-to-leading order (NLO) theoretical predictions. This procedure has met with great success showing general agreement between theory and experiment. To learn more about strong interactions it is now necessary to augment these old techniques with new ones where we probe QCD at higher rapidities and relatively lower p_T 's where we may begin to be sensitive to higher order effects. The DØ detector is uniquely qualified to carry out such studies with its hermetic calorimetric coverage. This note will describe one such analysis where we look for higher order effects by studying correlations between jets with large rapidity separations. By exploring the decorrelations of these jets we will learn about the interjet radiation patterns corresponding to these higher order QCD effects.

2 Theoretical Motivation

Fixed order perturbative expansions predict a finite amount of radiaton between the two jets comprising a dijet system, e.g., leading order (LO) has no radiation while next-to-leading order (NLO) allows one additional gluon in the system(Fig. 1). However, as the rapidity interval describing the dijet system increases and more gluons are emitted into the interval corresponding to higher order effects it is reasonable to assume that these limited descriptions of the radiation will eventually be insufficient.

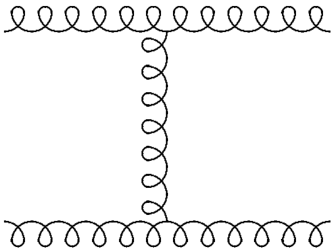

Figure 1: Feynman diagram representing leading order perturbative calculation.

1

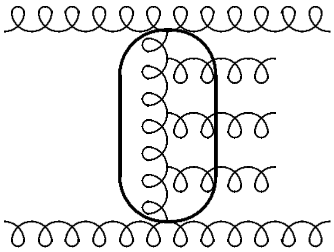

Figure 2: Feynman diagram representing BFKL radiation. The resummed gluons are indicated in the oval.

1

We consider in this analysis two different types of resummation, one based on GLAP evolution and the other on BFKL evolution. To model GLAP resummation we will use the HERWIG Monte Carlo. HERWIG produces this resummation through angular ordering of the final state radiation. This technique is equivalent to the resummation of soft gluon emission. The other type of resummation employs BFKL evolution. This was initially motivated by considering dijet production at very large rapidity intervals. Del Duca and Schmidt[1] along with Stirling[2] have shown that as the rapidity interval increases, large logarithms involving the now disparate scales describing the dijet production, i.e. $\hat{s} \gg Q^2$, become large invalidating the standard perturbative expansion in α_s . These logarithms correspond to gluon emission (Fig. 2). They employ the BFKL equation to resum these large logs to all orders in α_s and in effect resum these gluons. These two calculations differ in the terms that they resum.

3 Event Reconstruction and Selection Cuts

This analysis employed the JET_LOW trigger from run 1a. This trigger required one trigger tower (0.2×0.2 in η–ϕ) above 7 GeV and a z vertex within 10 cm of nomianl at level 1 (L1) and one jet with a cone of 0.7 above 30 GeV at level 2 (L2). For run 1a the L1 calorimeter trigger was implemented out to $|\eta| \leq 3.2$. This also limits L2 as a L1 seed tower is required to find a L2 jet. Although the trigger ran for most of the run, it was heavily prescaled so that only $\sim 137nb^{-1}$ was written to tape.

Trigger studies done using *mark and pass* runs, runs where all events that pass L1 are written to tape regardless of whether they pass L2, show that this trigger was efficient for finding jets with $\mathrm{E}_T^{uncorrected} > 40$ GeV[3]. This result confirms earlier Monte Carlo studies[4]. The study using *mark and pass* runs investigated the trigger in three different η regions: $0.0 < |\eta| < 0.6$, $0.6 < |\eta| < 1.6$ and $1.6 < |\eta| < 4.0$. Figure 3 shows the efficiency of the L1 term is plotted vs. $\mathrm{E}_T^{uncorrected}$ for three different η bins as well as integrated over the entire range. For each η region the trigger is $\sim 95\%$ efficient for $\mathrm{E}_T^{uncorrected} > 40$ GeV with some degradation in the intercryostat region ($\sim 90\%$). In Fig. 4 the efficiency of the L2 term is plotted vs. $\mathrm{E}_T^{uncorrected}$ for the same three η regions. We see here that the L2 trigger is almost 100% efficient by $\mathrm{E}_T^{uncorrected} = 40$ GeV. In Fig. 5 the combined L1 and L2 efficiencies are plotted for the same η regions. The central and forward η regions are $\sim 95\%$ efficient while the intercryostat region has a somewhat degraded efficiency ($\sim 90\%$) by $\mathrm{E}_T^{uncorrected} = 40$ GeV. At this point, no correction for trigger efficiency is made.

This data was reconstructed using RECO v10 and the standard correction algorithms. Jets were reconstructed offline using the standard cone algorithm with a radius of $R \leq 0.7$ in $\eta - \phi$ space, a seed and precluster threshold of 1 GeV and a minimum E_T^{jet} of 8 GeV[5]. Standard splitting and merging was enabled. The original Monte Carlo study performed using ISAJET and GEANT showed that this algorithm was essentially 100% efficient for reconstructing jets with $\mathrm{E}_T > 20$ GeV[6]. Subsequent data–based analyses have shown similar results setting a lower limit of 95% for jets with $\mathrm{E}_T^{corrected} > 20$ GeV[7, 8]. Efforts are underway to extend this data–based method as a function of rapidity. We have extended the original Monte Carlo study binning in rapidity and using HERWIG in place of ISAJET. The results of this study are shown in Fig.6. This study shows no loss of efficiency in the forward region.

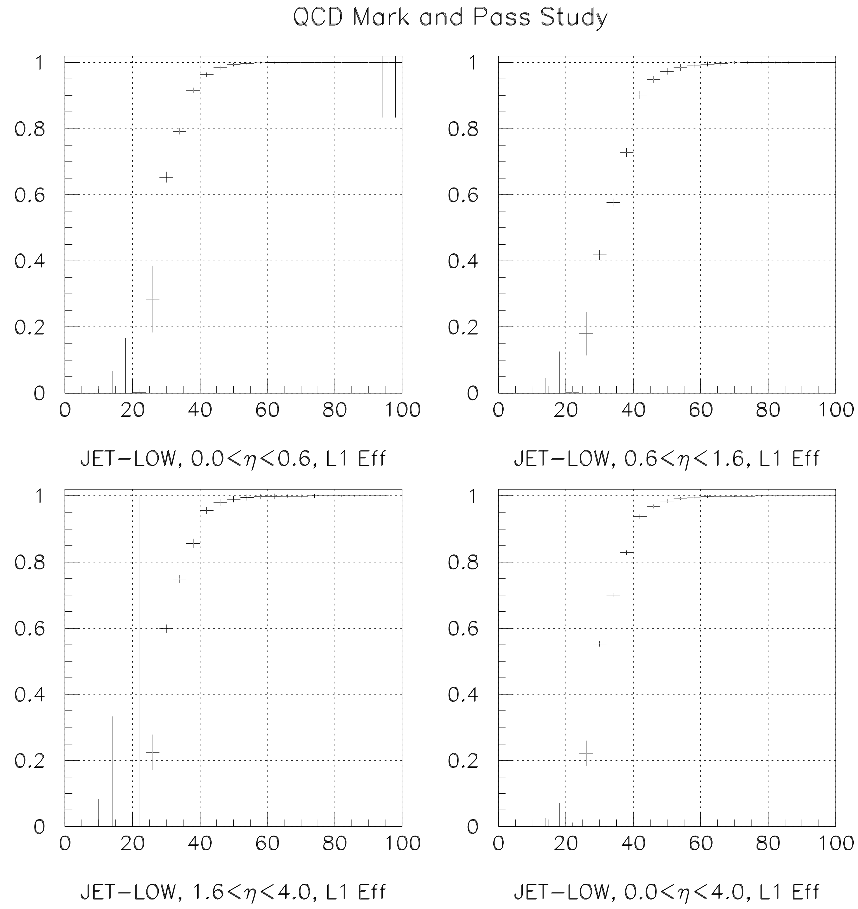

Figure 3: Level 1 trigger efficiency vs. E_T for the JET_LOW trigger for three different η regions and over all η. Courtesy of Terry Geld[3].

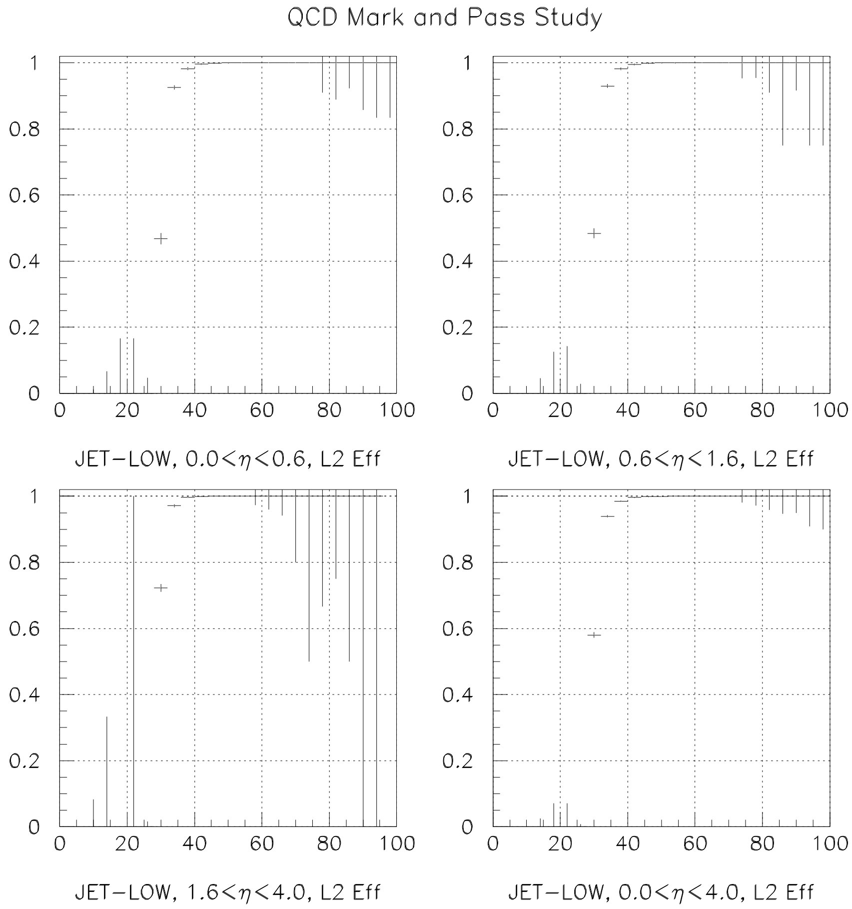

Figure 4: Level 2 trigger efficiency vs. E_T for the JET_LOW trigger for three different η regions and over all η. Courtesy of Terry Geld[3].

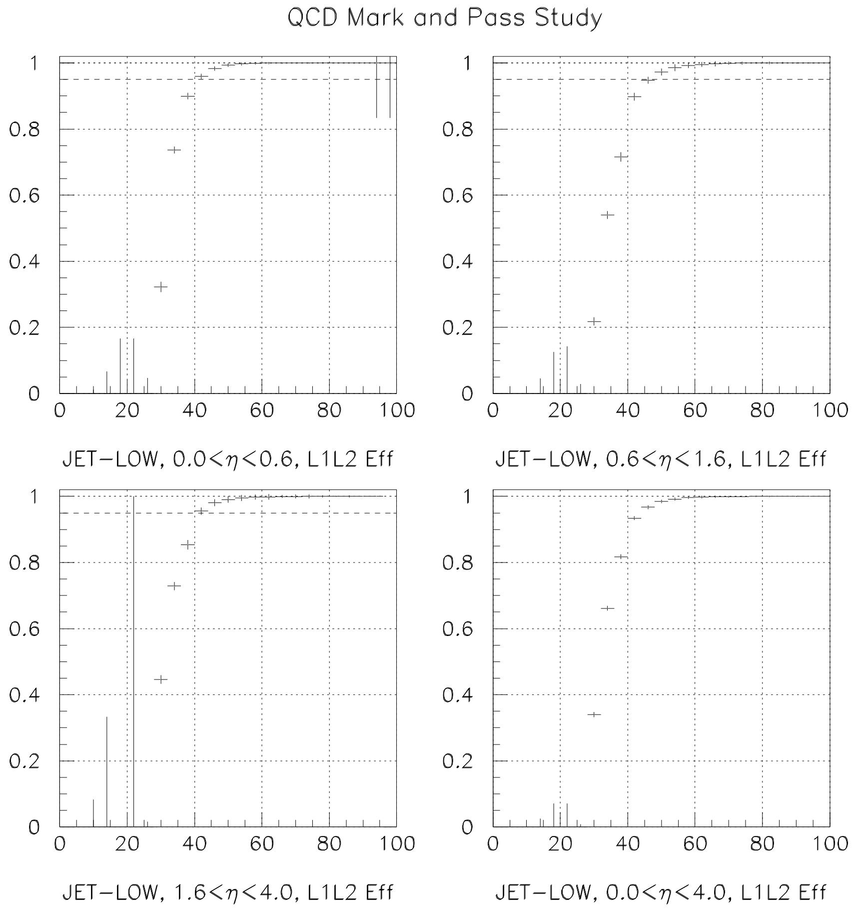

Figure 5: The combined level 1 and level 2 trigger efficiency vs. E_T for the JET_LOW trigger for three different η regions and over all η. Courtesy of Terry Geld[3].

Table 1: Reconstruction efficiencies calculated using HERWIG. Parton jets are matched with jets at the calorimeter level.

η	number of parton jets	calorimeter jets found	efficiency (%)	error (%)
-3.8	11	11	100	7.1
-3.4	61	61	100	1.6
-3.0	195	195	100	0.5
-2.6	474	471	99.4	0.4
-2.2	856	852	99.5	0.3
-1.8	1438	1430	99.4	0.2
-1.4	2057	2044	99.4	0.2
-1.0	2969	2953	99.5	0.1
-0.6	4024	4008	99.6	0.1
-0.2	4686	4660	99.4	0.1
0.2	4745	4722	99.5	0.1
0.6	4070	4047	99.4	0.1
1.0	3008	2994	99.5	0.1
1.4	2040	2030	99.5	0.2
1.8	1400	1395	99.6	0.2
2.2	806	798	99.0	0.4
2.6	464	462	99.6	0.4
3.0	188	186	98.9	0.9
3.4	62	62	100	1.5
3.8	5	4	80.0	16.0

The efficiencies and errors are given in Tab. 1.

The hadronic energy scale is tied to the electromagnetic energy scale. In the central region ($|\eta| \leq 1.0$) we determine the hadronic scale by minimizing the $\not{E}_T$ in direct photon events where photon energy has been scaled by the appropriate electromagnetic energy correction to make our Z mass agree with that of LEP. In the forward regions dijet E_T balancing is used[9]. For this study we used QCD_JET_CORRECTION v4.0 using all corrections (out–of–cone, zero–suppression, underlying–event) scaling a typical jet upwards in E_T by $\sim 20\%$[10]. This in combination with the L2 trigger efficiency is what will determine our final offline E_T cuts.

Spurious jets were removed using the standard QCD bad jet cuts. These

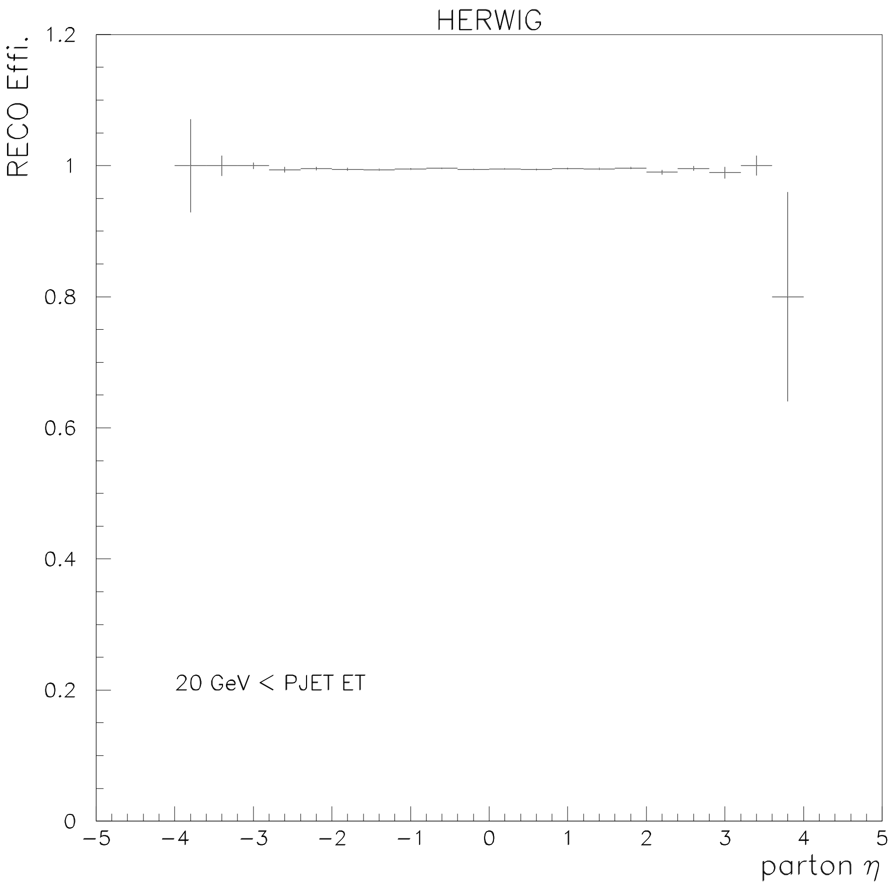

Figure 6: Results from the HERWIG reco study.

cuts include the electromagnetic energy fraction of the jet ($0.05 < \mathrm{EMF} < 0.95$), the ratio of the energy of the second most energetic jet cell to the most energetic cell in the jet ($\mathrm{HCF} > 0.1$) and the coarse hadronic energy fraction ($\mathrm{CHF} < 0.40$). These cuts are designed to remove fake jets that are the result of electronic noise or energy not deposited by particles eminating from the $\overline{p}p$ collision. These cuts are greater than 95% efficient for the E_T and η regions of interest while rejecting more than 90% of bad jets[11, 12, 13]. All three cuts were applied over all η except for the EMF cut which was not applied in the intercryostat region (ICR) where there was no electromagnetic calorimetry ($\mathrm{EMF} < 0.95 : 1.0 < |\eta| < 1.6$).

The remaining jets are then orderd in rapidity after a E_T^{min} cut of 20 GeV is applied. We then locate the jet pair with the largest rapidity interval in the event ($\Delta\eta = \eta_1 - \eta_2$) labelling the most forward jet J_1 and the most backward jet J_2. Due to possible reconstruction inefficiencies we do not consider jets with with $|\eta_{jet}| > 3.0$. To ensure that there is no trigger bias we require either J_1 or J_2 to have sufficient E_T to efficiently fire the trigger ($\mathrm{E}_T^{corrected} > 50$ GeV) and be in the η region efficiently covered by the L1 trigger ($|\eta^{detector}| < 3.0$)[3]. To ensure complete acceptance and reasonable values of x we then require $|\bar{\eta}| = |\frac{\eta_1+\eta_2}{2}| < 0.5$. The remaining events are then binned in unit bins of $\Delta\eta$ centered on integral values of $\Delta\eta$ (e.g. for $\Delta\eta = 2$: $1.5 \leq \Delta\eta < 2.5$). We are concerned with $dN/d\Delta\eta$, $dN/d\Delta\phi$ for various $\Delta\eta$ where $\Delta\phi = \pi - (\phi_1 - \phi_2)$, and $< \cos\, \Delta\phi >$ vs. $\Delta\eta$. The last distribution should provide some ability to distinguish between various theoretical predictions and our experimental results.

4 Monte Carlo

The Monte Carlos used in this analysis perform two functions. First of all they provide us with various predictions using different theoretical assumptions. JETRAD[14] is a parton level Monte Carlo simulation package which includes next-to-leading order (α_s^3) for 2 to 2 parton processes (including loops) and leading order (α_s^3) for 2 to 3 parton processes. Since it is a next-to-leading order (NLO) parton generator it can at most have three jets in the final state. This will probably be inadequate to describe events when the average jet multiplicity exceeds this. HERWIG[15] is a parton shower simulation where higher order effects are approximated by the parton shower which is superimposed on a leading order 2 to 2 parton process. The higher order effects are implemented through angular ordering (radiation of each subsequent gluon is always at a smaller relative angle than the previous radiation). This will in effect resum certain types of soft gluon radiation where the resummation is governed by the GLAP equation. HERWIG has very successfully described various jet distributions in the past including the recent DØ jet shape. Secondly we use the Monte Carlos to understand various theoretical and experimental systematic errors(Sec. 5).

In our JETRAD analysis we typically would generate more than 100 million events to smooth out the effects of negative cross section produced by virtual corrections and divergences due to soft and collinear gluon radiation (e.g. jets back to back in ϕ). Jets were generated with a E_T^{min} of 17 GeV and a E_T^{max} of 400 GeV between the rapidities of -4 and 4 to remove any biases from phase space edges. For our HERWIG analysis we typically generated on the order of 50,000 events with a E_T^{min} of 10 GeV and a E_T^{max} of 400 GeV with very loose constraints on the rapidity (-8 to 8).

In the future we plan to expand our efforts with Monte Carlos. This will include examining additional event generators including PYTHIA and ISAJET. In addition a larger sample of HERWIG events will be generated and process through D0GEANT. This will allow us to do systematic studies comparing parton, particle and calorimeter level simulations.

5 Systematic Errors

Sources of systematic errors in this study include η and ϕ resolutions, poorer jet energy resolution in the ICR, energy scale uncertainties both in overall scale and uncertainties in the forward region, showering effects in the calorimeter and jet cone size dependencies. The largest effects are seen the jet energy scale uncertainties.

The error on $< \cos(\pi - \Delta\phi) >$ is the variance of the $\cos(\pi - \Delta\phi)$ distribution for the ensemble used, which corresponds to the uncertainty of expectation value for the arithmatic average of $\cos(\pi - \Delta\phi)$. On the other hand, the error due to the position resolution of jet finding is estimated semi-analytically by using the event distribution in $\Delta\eta - \Delta\phi$ space. It is assumed that the normalized distribution is a true probablilty distribution of the dijet events in the given $\Delta\eta - \Delta\phi$ configuration. Then the error due to $\Delta\eta$ and

$\Delta\phi$ resolutions which are characterized by the η and ϕ resolutions is obtained by a variational method with the probability distribution.

We explored the effects on our studies of the energy scale by repeating all of our analyses using the high and low correction values available in QCD_JET_CORRECTION. The same 20 GeV E_T^{min} cut was then applied to the rescaled jets. In addition to the hi/lo corrections, we investigated the effects of the out–of–cone correction in the forward region. We reprocessed the data turning off the out–of–cone correction for all η (Fig. 7). No large effects were seen and only small shifts in the $\Delta\eta = 2$ and 3 bins.

Effects of jet reconstruction efficiency and energy resolution in the ICR were investigated. Plotted in Fig. 8 is the detector η distribution of the jets that were used in this analysis for all $\Delta\eta$ and for individual $\Delta\eta$ in Fig. 9. The excess of events with jets in the ICR can be seen for both the forward and the backward jets. To investigate any effects these events may have on the analysis, we repeated the analysis removing any events where either the forward or the backward jet was in the ICR ($1.0 < |\eta| < 1.4$). A comparison of the two different results are shown in Fig. 10. We will quote the shift in value as a systematic error. We also investigated the effect the the jet quality cuts in general. We repeated the analysis retaining all jets that failed the cuts and quote the shift as a systematic error (Fig. 11). The η bias correction was also studied. We show the results with and without the correction applied (Fig. 12).

Effects of fragmentation, hadronization and calorimeter showering were also investigated. We used a sample of events generated using HERWIG and run through GEANT. We then compared results at the parton, particle and calorimeter level as a function of $\Delta\eta$ using 0.7 cones. Additional statistics will help to reduce the error on this study. We do not feel comfortable at this quoting either a correction or an error for the large $\Delta\eta$ regions(Fig. 13).

A summary of the statistical and systematic errors for each of the above effects is shown below (Tab. 2).

6 Results and Prospects

In fig. 14 we plot the E_T distributions of the jets we use in the analysis. The first plot shows the jet that is required to be above the trigger threshold while the second shows the jet required to be above the reconstruction threshold.

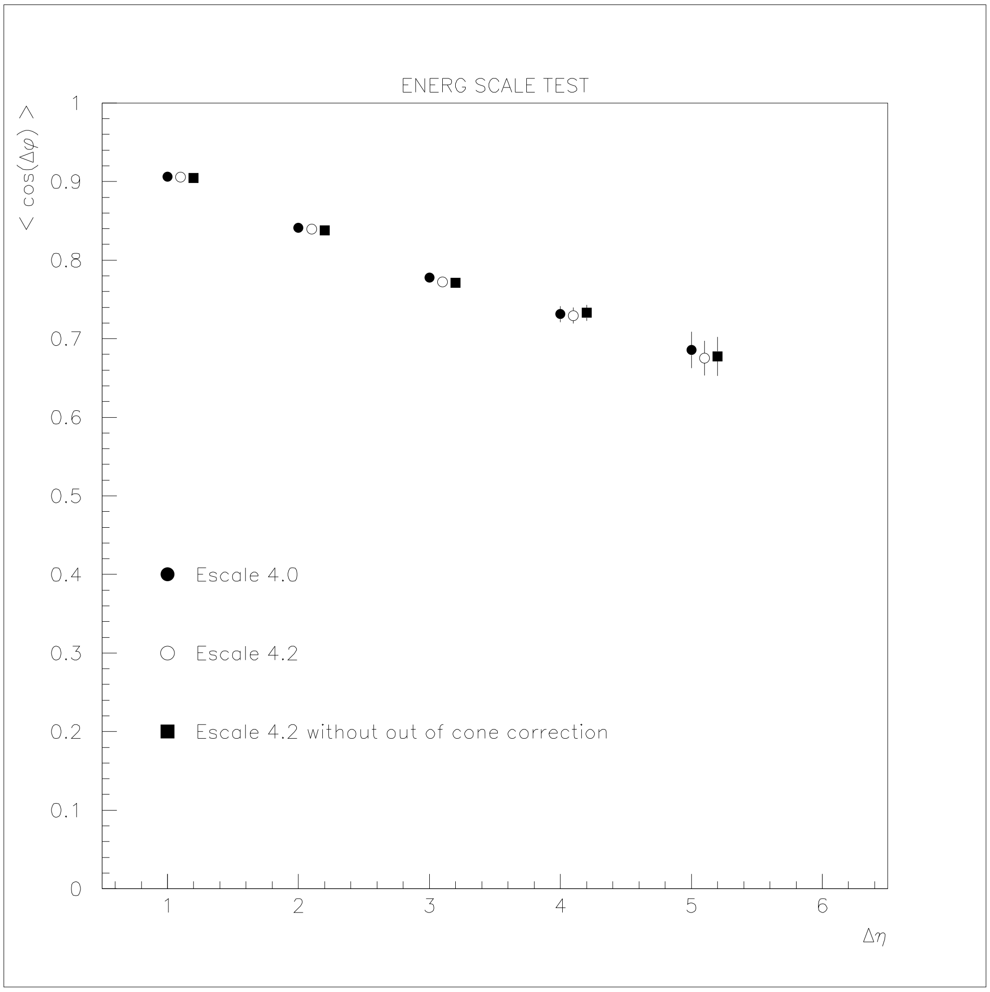

Figure 7: Effects of different energy scale assumptions.

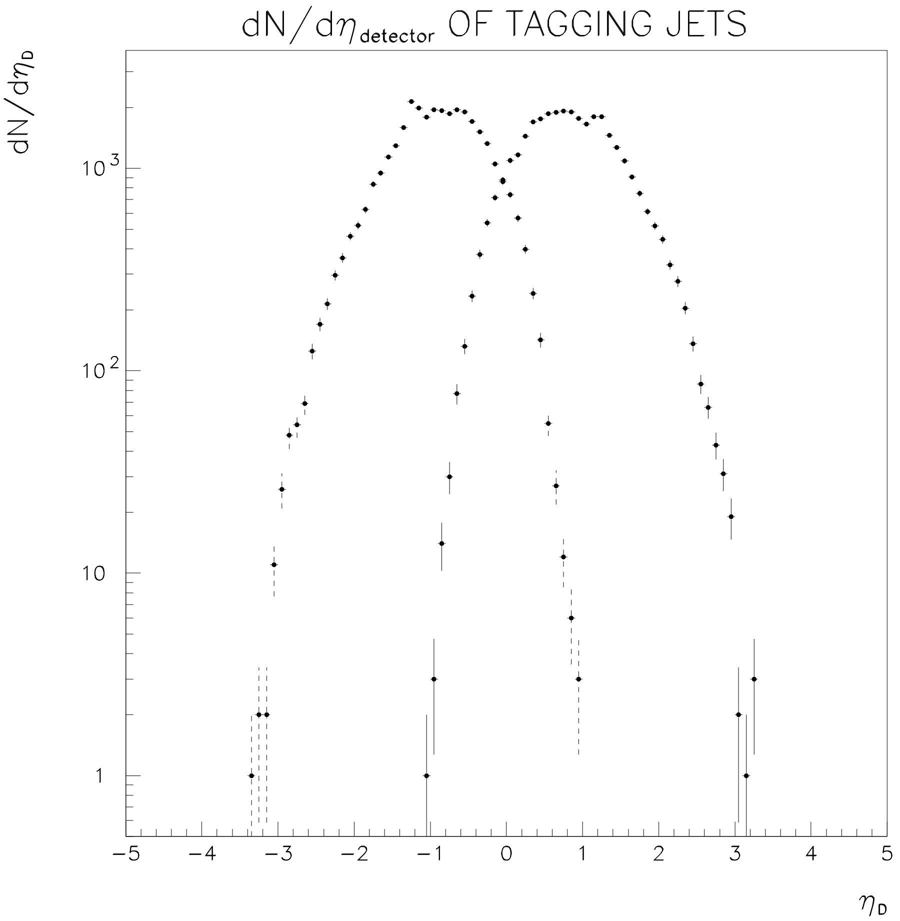

Figure 8: η distribution of the tagging jets, one for the forward jets and one for the backward jets.

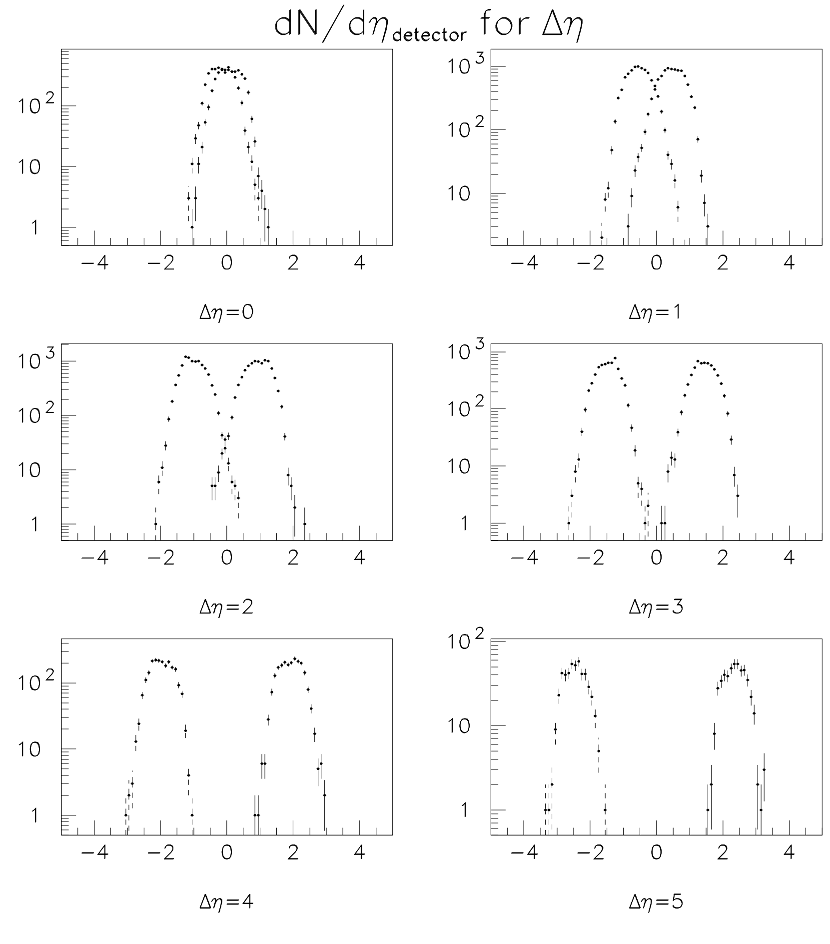

Figure 9: η distributions of the tagging jets for individual $\Delta\eta$.

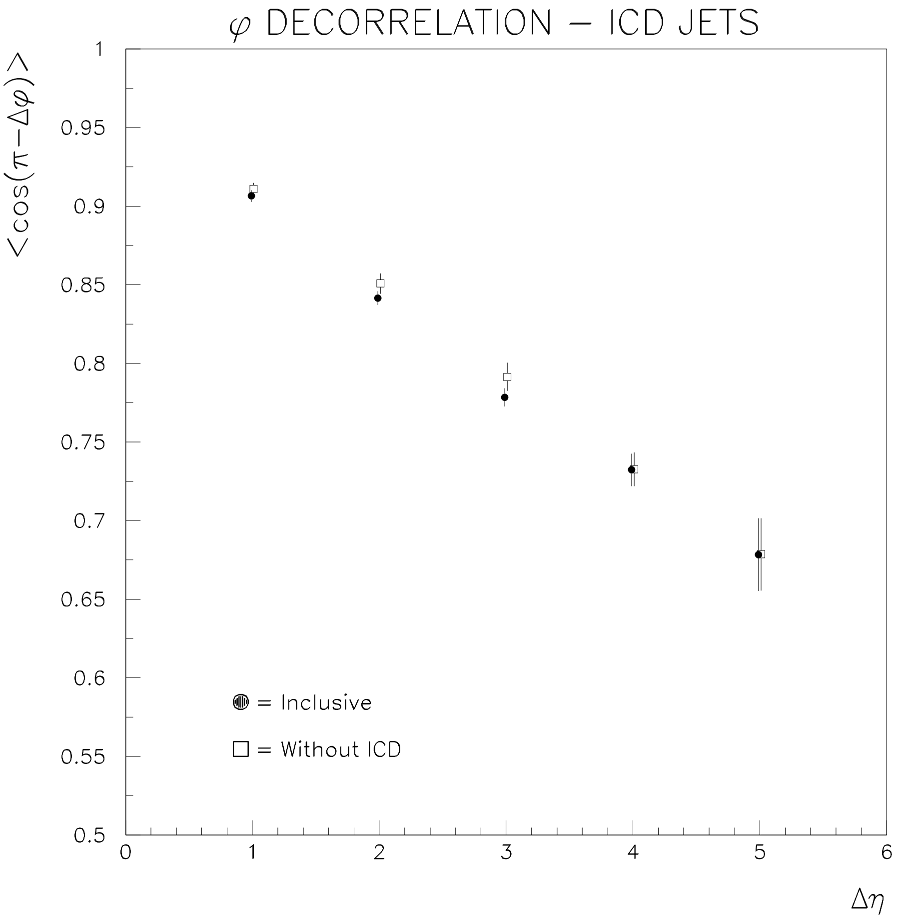

Figure 10: $<\cos(\pi-\Delta\phi)>$ with and without the ICR jets.

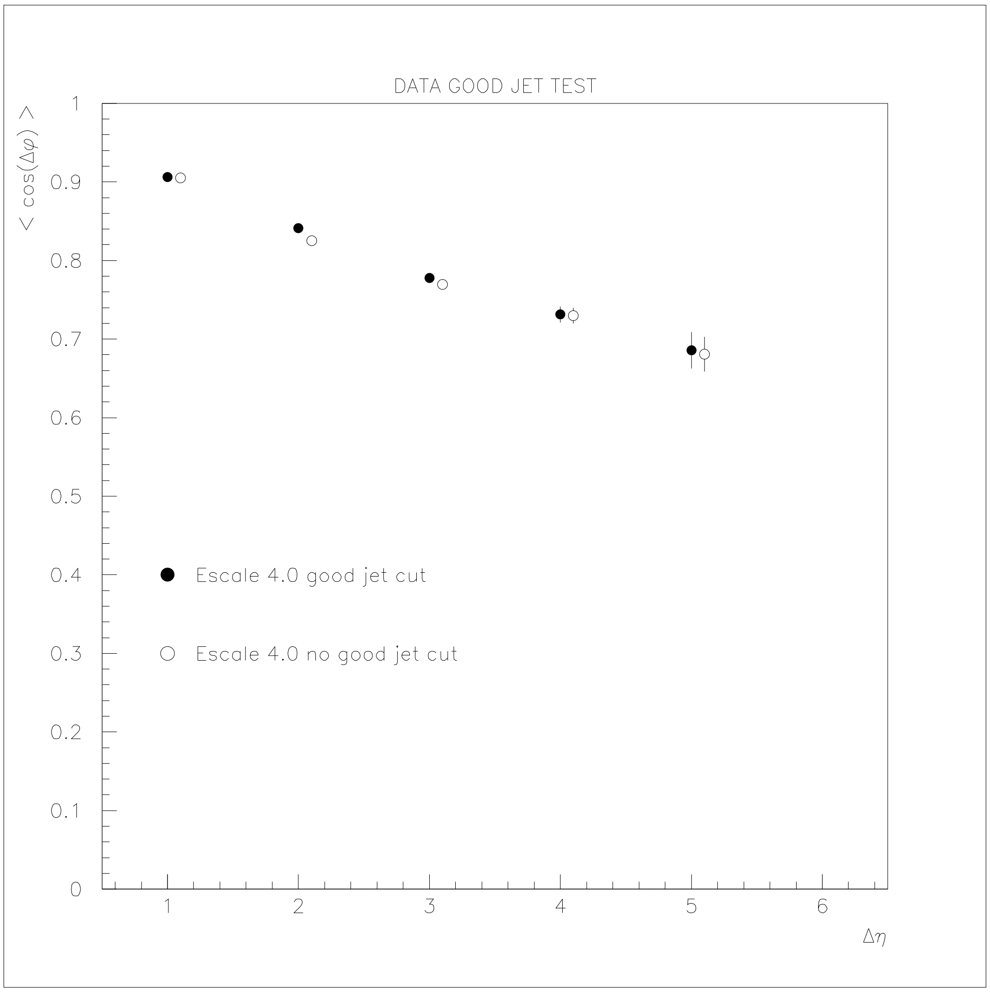

Figure 11: $< \cos(\pi - \Delta\phi) >$ with and without jet quality cuts.

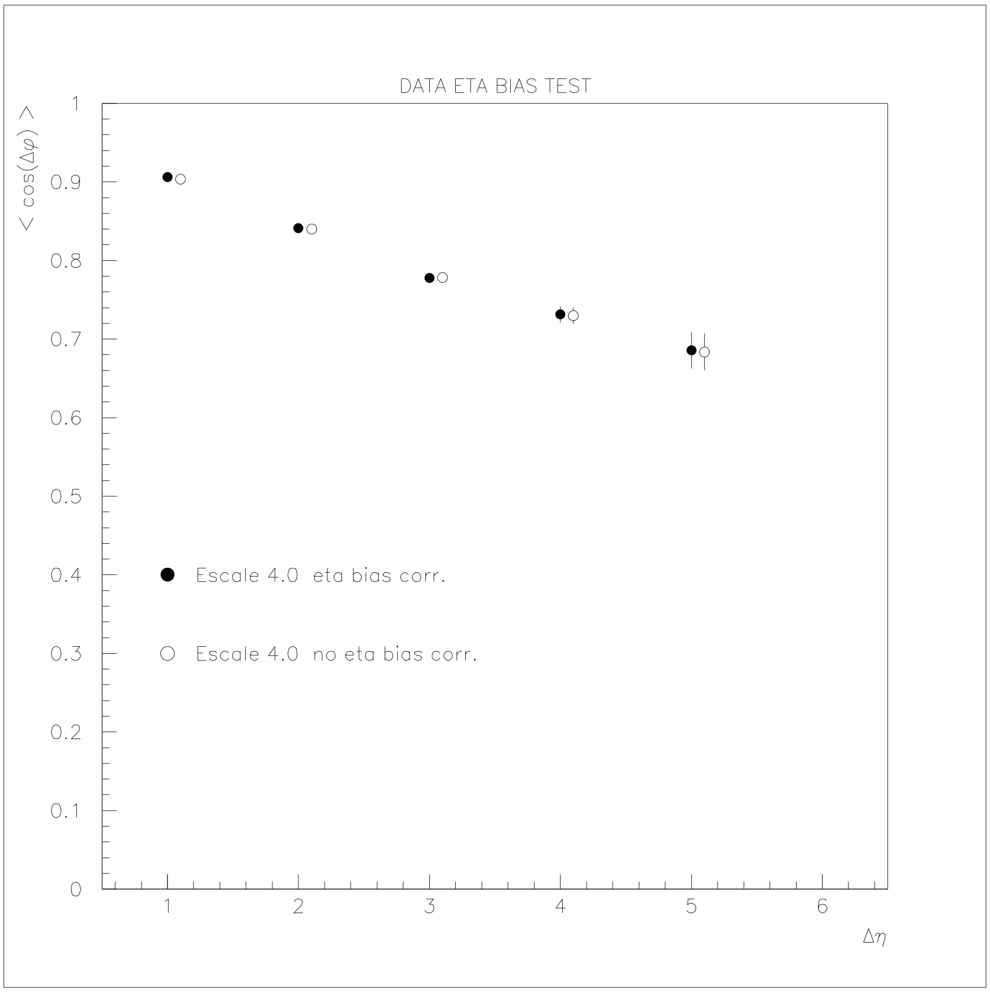

Figure 12: $< \cos(\pi - \Delta\phi) >$ with and without η bias correction.

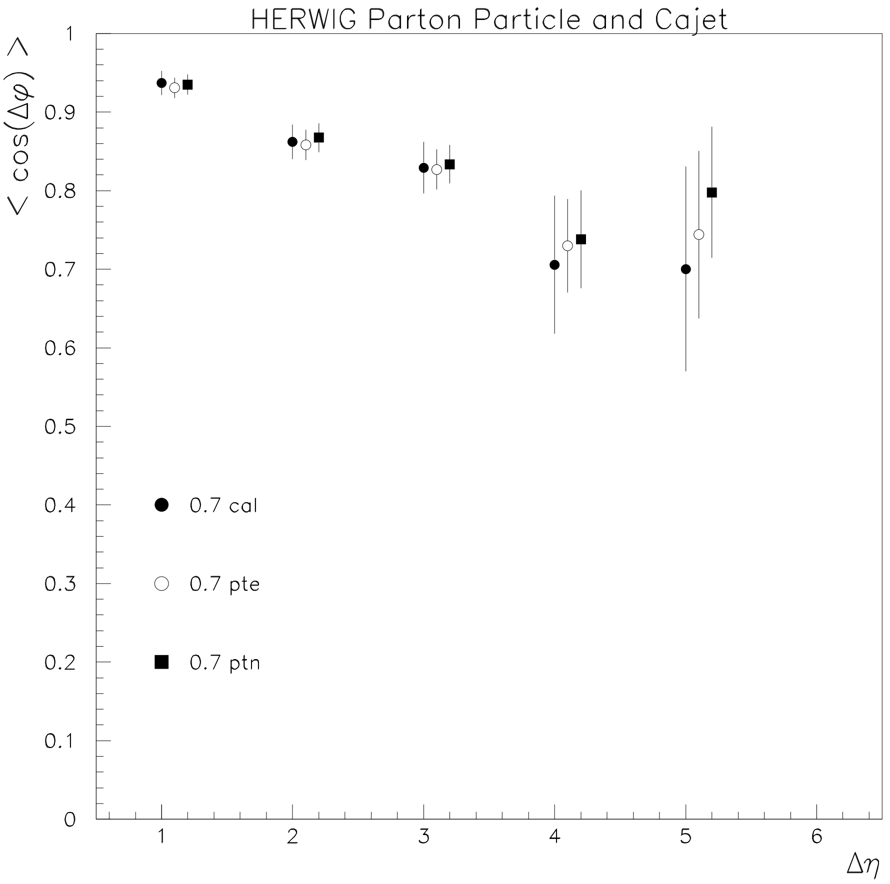

Figure 13: $< \cos(\pi - \Delta\phi) >$ vs $\Delta\eta$ for HERWIG at the parton, particle and calorimeter levels.

Table 2: Summary of statistical and systematic errors in the determination of $< \cos(\pi - \Delta\phi) >$.

$\Delta\eta$	1	2	3	4	5
$< \cos(\pi - \Delta\phi) >$	0.906	0.842	0.778	0.732	0.678
statistical	0.003	0.004	0.005	0.010	0.023
ϕ resolution	0.001	0.001	0.001	0.001	0.001
η resolution	0.002	0.002	0.002	0.002	0.002
out–of–cone correction	0.000	0.001	0.001	0.004	0.003
energy scale	0.006	0.011	0.012	0.012	0.010
energy scale (v4.0 vs v4.2)	0.001	0.002	0.006	0.002	0.011
jet quality cuts	0.001	0.016	0.008	0.001	0.005
reconstruction in ICR	0.005	0.009	0.013	0.004	0.000
η bias correction	0.003	0.001	0.000	0.001	0.002
renormalization scale	0.002	0.003	0.004	0.006	0.015
parton distribution function	0.002	0.002	0.003	0.006	0.014
total systematic	0.009	0.022	0.021	0.016	0.026

In addition we show the η distributions of these jets in Fig. 8 for all $\Delta\eta$ and for individual $\Delta\eta$ in Fig. 9. This shows some excess of events in the ICR region. We also include the plot of the multiplicity distribution in Fig. 15. The plot shows that there are indeed a large number of events with more than three jets.

In Fig. 17 we plot the $\Delta\eta$ distribution for our events spanning $0 < \Delta\eta < 6$. Although this plot is not corrected for efficiencies and acceptances and is not a true cross section we see that the number of events falls very rapidly with $\Delta\eta$. In this study we are able to extend our coverage out to $\Delta\eta = 5$. In run 1b we expect to use the improved η coverage of the trigger to extend this out to $\Delta\eta = 6$.

In Fig. 18 we plot the $\Delta\phi$ distributions for jets in three $\Delta\eta$ bins: $\Delta\eta = 1$, 3 and 5. Each distribution is normalized to unit area. We can see in this plot that as we increase $\Delta\eta$, the peak of the $\Delta\phi$ distribution decreases while more events end up in the tails. This suggests that there is some decorrelation in ϕ occurring.

In Fig. 19 we plot the $< \cos(\pi - \Delta\phi) >$ distribution as a function of $\Delta\eta$. We include results from our data, JETRAD, HERWIG and BFKLpredictions

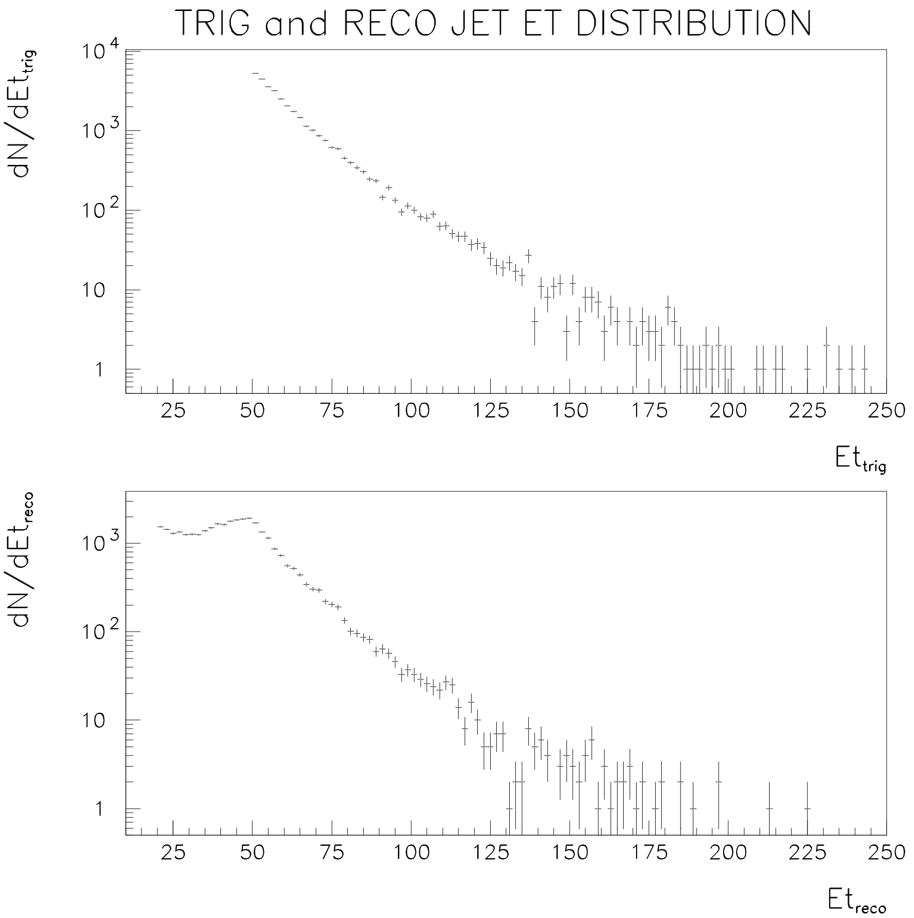

Figure 14: E_T distributions of tagging jets used in the analysis.

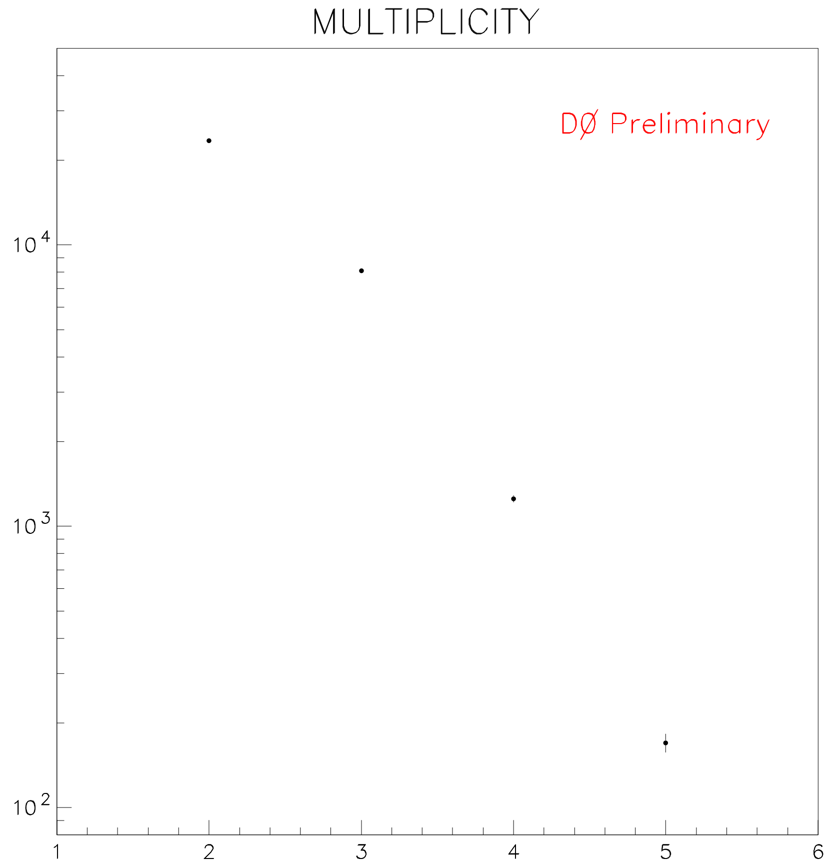

Figure 15: Multiplicity distribution of jets (dN/dN_{jets}).

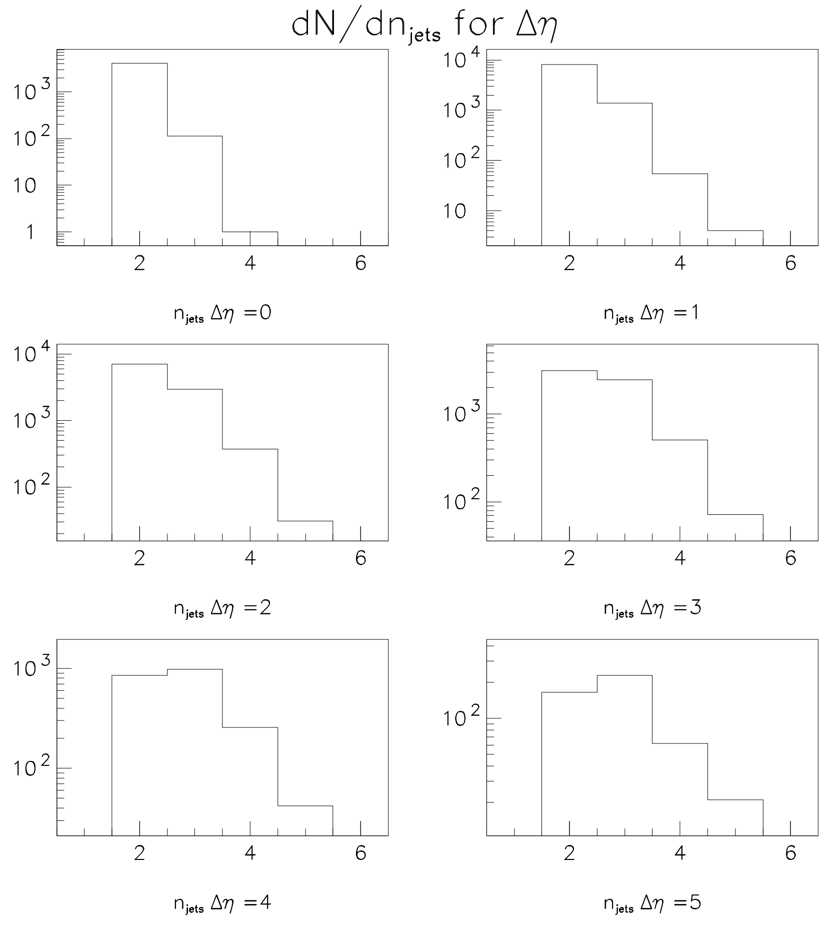

Figure 16: Multiplicity distribution of jets (dN/dN_{jets}) for each $\Delta\eta$.

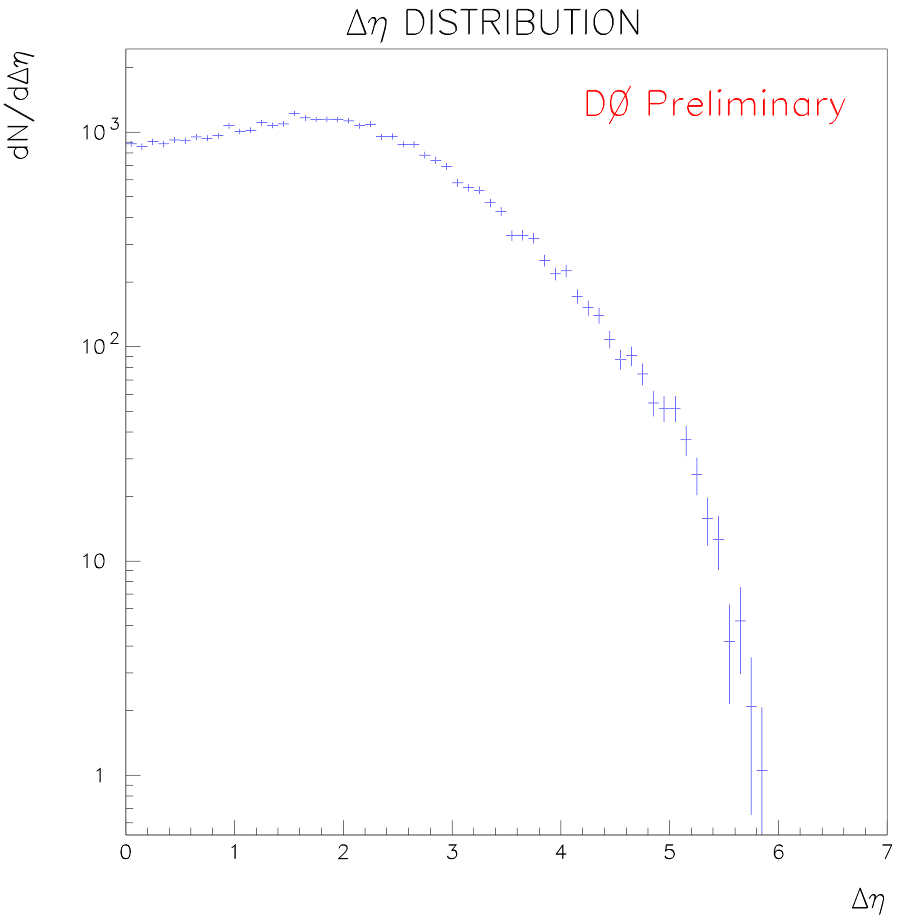

Figure 17: $\Delta\eta$ distribution (dN/d$\Delta\eta$).

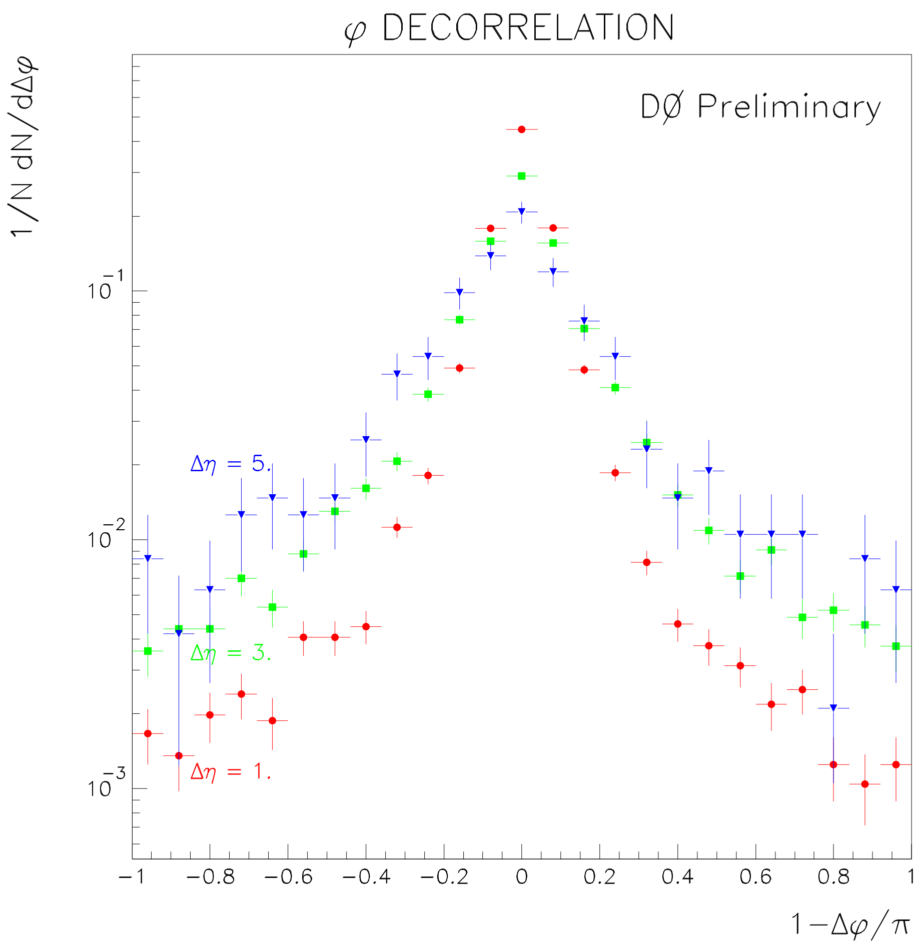

Figure 18: $\Delta\phi$ distribution $(dN/d\Delta\phi)$ for $\Delta\eta = 1$, 3 and 5.

of Del Duca and Schmidt. We see in these plots that the data does show substantial decorrelation in ϕ as demonstrated by the curve tending lower as a function of $\Delta\eta$. It is apparent that JETRAD does not describe the data very well while HERWIG even without calorimeter simulation does a reasonably good job. Although the BFKL prediciton shows the proper trend in decorrelation, it tends to overestimate the amount present.

7 Conclusions

We have measured jet decorrelation in ϕ as a function of $\Delta\eta$. This allows us to study resummation effects as well as learn about the general behavior of jets with large rapidity separation. We see that these jets do indeed decorrelate with $\Delta\eta$. Although JETRAD does not reproduce the data, predicting too little decorrelation, HERWIG with its angular ordering resummation approximation seems to be able to predict the relative amount of decorrelation as well as the absolute amount of decorrelation. BFKL shows the proper trend in relative decorrelation, but tends to overestimate the absolute amount of decorrelation.

References

[1] V. Del Duca and C.R. Schmidt, 'Dijet Production at Large Rapidity Intervals', Phys. Rev. D **49**, 4510 (1994); preprint DESY 94-144 (1994).

[2] W.J. Stirling, 'Production of Jet Pairs at Large Relative Rapidity in Hadron-Hadron Collisions as a Probe of the Perturbative Pomeron', Nucl.Phys.**B428**: 3-18, 1994.

[3] T.L. Geld, 'Trigger Efficiencies for Run 1A Inclusive Jet Triggers', DØNote 2474, February 9, 1995.

[4] R.V. Astur and A. Milder, 'Jet Trigger Efficiency in the DØ Detector', DØNote 1663, March 8, 1993.

[5] N. Hadley, 'Cone Algorithm for Jet Finding', DØNote 904, November 28, 1989.

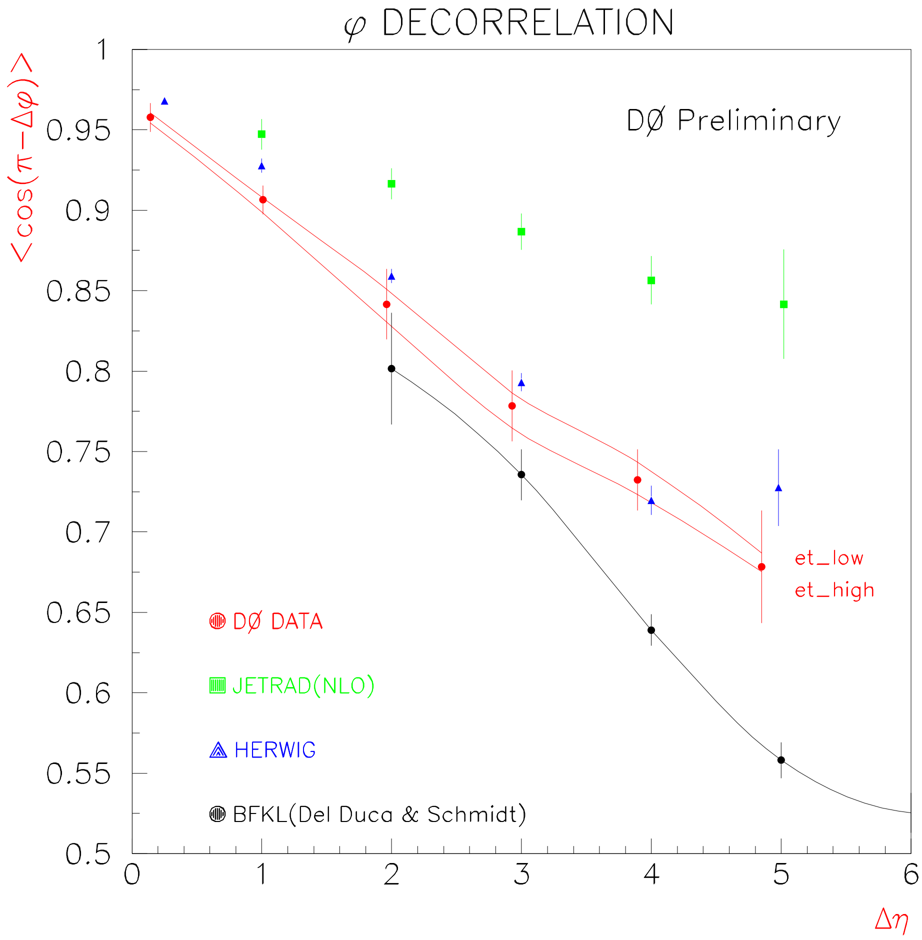

Figure 19: $< \cos(\pi - \Delta\phi) >$ vs. $\Delta\eta$ for JETRAD, HERWIG, BFKL and data.

[6] A. Milder, 'Dijet Angular Distributions at $\sqrt{s} = 1800$ GeV using the DØ Detector', DØNote 1874, October 14, 1993.

[7] R. Hirosky, 'A Data–based Estimate of Jet Reconstruction Efficiencies', DØNote 2369, November 1994.

[8] R. Hirosky, 'Jet Efficiencies and Seed Tower Distributions in the DØ Cone Algorithm', DØNote 2405, January 1994.

[9] A. Milder and R.V. Astur, 'Jet Energy Calibration Using the Missing E_T Projection Fraction', DØNote 1657, March 30, 1993.

[10] R.V. Astur, 'Energy Scale Corrections', DØNote 2089, March 21, 1994.

[11] R.V. Astur, 'Study of Fake Jets in the DØ Detector', DØNote 1662, March 20, 1993.

[12] V.D. Elvira, G. Blazey and R.V. Astur, 'A study of Standard Jet Cuts and their Efficiencies Using DØ Collider Data', DØNote 1763, June 21, 1993.

[13] M Bhattacharjee, V.D. Elvira and G. Blazey, 'Efficiencies of the Standard Jet Cus for Cone Sizes: 0.3, 0.5, 0.7', DØNote 2197, Jully 15, 1994.

[14] W.T. Giele, E.W.N. Glover and D.A. Kosower, Nucl. Phys. **B403**, 633 (1993).

[15] G.Marchesini and B.R.Webber, Nucl. Phys. **B310**, 461 (1988).